Published in final edited form as:
J Am Chem Soc. 2008 December 31; 130(52): 17826–17835. doi:10.1021/ja805940m.

The amyloid-β peptide of Alzheimer's disease binds Cu^{I} in a linear bis-His coordination environment: Insight into a possible neuroprotective mechanism for the amyloid-β peptide

Jason Shearer[1] and **Veronika A. Szalai**[2]

Jason Shearer: shearer@unr.edu; Veronika A. Szalai: vszalai@umbc.edu

[1]Department of Chemistry/216, University of Nevada-Reno, 1664 N. Virginia St, Reno, NV 89557

[2]Department of Chemistry & Biochemistry, University of Maryland Baltimore County, 1000 Hilltop Circle, Baltimore, MD 21250

Abstract

Oxidative stress has been suggested to contribute to neuronal apoptosis associated with Alzheimer's disease (AD). Copper may participate in oxidative stress through redox-cycling between its +2 and +1 oxidation states to generate reactive oxygen species (ROS). In vitro, copper binds to the amyloid-β peptide of AD and in vivo, copper is associated with amyloid plaques characteristic of AD. As a result, the $A\beta Cu^{I}$ complex may be a critical reactant involved in ROS associated with AD etiology. To characterize the $A\beta Cu^{I}$ complex, we have pursued X-ray absorption (XAS) and EPR spectroscopy of $A\beta Cu^{II}$ and $A\beta Cu^{I}$ (produced by ascorbate reduction of $A\beta Cu^{II}$). The $A\beta Cu^{II}$ complex Cu K-edge X-ray absorption spectrum is indicative of a square-planar Cu^{II} center with mixed N/O ligation. Multiple scattering analysis of the extended X-ray absorption fine structure (EXAFS) data for $A\beta Cu^{II}$ indicate that two of the ligands are imidazole groups of histidine ligands, indicating a $(N_{Im})_2(N/O)_2$ Cu^{II} ligation sphere for $A\beta Cu^{II}$. After reduction of the $A\beta Cu^{II}$ complex with ascorbate, the edge region decreases by ~4 eV in energy. The X-ray absorption near-edge spectrum (XANES) region of $A\beta Cu^{I}$ displays an intense pre-edge feature at 8984.1(2) eV. EXAFS data fitting yielded a two coordinate geometry with two imidazole ligands coordinated to Cu^{I} at 1.877(2) Å in a linear geometry. Ascorbate reduction of $A\beta Cu^{II}$ under inert atmosphere and subsequent air oxidation of $A\beta Cu^{I}$ to regenerate $A\beta Cu^{II}$ was monitored by low-temperature EPR spectroscopy. Slow re-appearance of the $A\beta Cu^{II}$ EPR signal indicates that O_2 oxidation of the $A\beta Cu^{I}$ complex is kinetically sluggish, and Aβ damage is occurring following reoxidation of $A\beta Cu^{I}$ by O_2. Together, these results lead us to hypothesize that Cu^{I} is ligated by His13 and His14 in a linear coordination environment in Aβ, that Aβ may be playing a neuroprotective role, and that metal-mediated oxidative damage of Aβ occurs over multiple redox-cycles.

Introduction

Alzheimer's disease (AD) is a fatal neurodegenerative disorder that plagues approximately 26 million people worldwide.[1] AD is characterized by a progressive cognitive decline that has been attributed to the deposition of extracellular protein plaques containing the amyloid-β

Correspondence to: Jason Shearer, shearer@unr.edu; Veronika A. Szalai, vszalai@umbc.edu.

Supporting Information Available: XAS spectra of $A\beta 40Cu^{I}$, additional refinements to the EXAFS region of $A\beta 16Cu^{II}$ and $A\beta 16Cu^{I}$, EPR spectra of the reoxidation of $A\beta 16Cu^{I}$ by Ir(IV), reduction/air reoxidation of Aβ40CuII with excess ascorbate in anaerobic solution and in air-saturated buffer, digitized XAS data from Stellato et al.,[35] our re-refinement of EXAFS data from Stellato et al.,[35] geometry optimized structure for $(Cu^{I}(His)_2)+$, control HPLC and GPC chromatograms of air exposed $A\beta Cu^{II}$, and complete reference 51 are available free of charge via the Internet at http://pubs.acs.org.

(Aβ) peptide. A single determinant for AD etiology has not been established,[2,3] but oxidative stress induced by reactive oxygen species (ROS) has been hypothesized to be a principal contributor.[4] The redox-active metal ions iron and copper are found in AD plaques,[5] suggesting that they might mediate ROS generation.[6] Thus, answers to fundamental questions regarding the coordination environment and reactivity of these metal ions when bound to Aβ are essential to evaluating their potential role in AD etiology.

The majority of previous studies performed on copper-Aβ adducts were aimed at elucidating the coordination environment of Cu^{II} bound to the peptide.[6-11] Although some work has focused on the ROS reactions catalyzed by the AβCu complex,[10,12,13] information regarding the structure and reactivity of the $A\beta Cu^{I}$ complex is scarce.[14-16] Previous EXAFS measurements of $A\beta Cu^{II}$ led to a model in which the Cu^{II} ion binds to Aβ in a 5-coordinate square-pyramidal ligand environment created by coordination to three His imidazoles, an oxygen atom donor (Tyr), and an axial water molecule. Results from other XAS measurements proposed a 6-coordinate Cu^{II} species bound to three His imidazoles, Glu/Asp residues, and a water molecule.[17] These structural models are inconsistent with 4-coordinate Cu^{II} in the Cu^{II}–Aβ adduct, a geometry that has been suggested on the basis of other spectroscopic data and recent theoretical work.[8,9,18,19]

Recent XANES data indicated that the $A\beta Cu^{II}$ complex can be reduced by ascorbate and 6-hydroxydopamine, but not by cholesterol or dopamine.[15] In another study, Maiti et al. reduced the $A\beta Cu^{II}$ complex with sodium borohydride, a non-physiological reductant, and followed the reduction reaction with EPR and fluorescence spectroscopies.[14] Ascorbate radical and hydroxyl radical (either via fluorescent detection or spin-trapped adducts) have been detected upon redox-cycling of the AβCu system.[13,20] None of these authors generated the $A\beta Cu^{I}$ complex under inert atmosphere nor did they probe the O_2 reactivity of the $A\beta Cu^{I}$ complex over time.[14] Furthermore, quantification of the amount of $A\beta Cu^{II}$ produced following air-oxidation was never rigorously assessed.

Herein we present XAS data of both the $A\beta Cu^{II}$ and $A\beta Cu^{I}$ complexes along with EPR spectroscopic monitoring of the reduction and re-oxidation of the AβCu complex. These studies will demonstrate that the Cu^{I} ion forms a stable well defined adduct with Aβ. Furthermore, oxidation of Cu^{I} to Cu^{II} by O_2 is kinetically sluggish, yet none the less affords Aβ damage. The biological implications of these new findings and their implications for AD will be discussed.

Materials and Methods

Materials

Aβ40 and Aβ16 peptides were purchased from Bachem (King of Prussia, PA) or rPeptide (Athens, GA) or synthesized on a Protein Technologies PS3 peptide synthesizer using standard Fmoc chemistries and subsequently purified by HPLC as previously described.[11] The amino acid sequence for the Aβ40 peptide is DAEFRHDSGYEVHHQKLVFFAEDVGSNKGAIIGLMVGGVV; the amino acid sequence of Aβ16 is the first 16 amino acids of Aβ40. Biological grade glycerol, sodium phosphate, 1,1,1,3,3,3-hexafluoroisopropanol (HFIP), and sodium chloride were purchased from Fisher Scientific (Pittsburgh, PA). Bovine serum albumin (BSA) standards were purchased from Sigma-Aldrich (St. Louis, MO). Quartz EPR tubes were purchased from Wilmad (Buena, NJ). Solutions were prepared in MilliQ™ water (resistivity > 18 mΩ, total organic content < 35 ppb). Sodium ascorbate was purchased from Spectrum Chemicals (Gardena, CA). Na_2IrCl_6 was from Alfa-Aesar (Ward Hill, MA).

Sample Preparation

Aβ peptides were monomerized with HFIP and stored at -80 °C in HFIP as previously reported.[18,21] Peptide stock solution in HFIP was removed via a Hamilton gastight syringe that had been washed previously with multiple volumes of HFIP. An aliquot of the peptide stock in HFIP was removed for peptide concentration determination using a BSA calibration curve.[18,21] Immediately prior to making peptide samples, HFIP was removed using a spin-vacuum system. This protocol produces homogeneous solutions of monomeric peptide.[22]

Samples of soluble Aβ16 or Aβ40 were prepared by resuspending dried peptide into buffer containing 50 mM NaP_i, 75 mM NaCl, pH 7.2 with 50% glycerol (v/v). The Aβ16 peptide was used to model Cu(II) binding to soluble Aβ because it is well-established that this region contains the Aβ Cu-binding domain[8,9,18,23] and because it does not contain the fibrillization domain (residues 17-21).[23]

Cu^{II} stock solutions were generated as previously reported.[18,21,24] The Cu^{II} concentration in each EPR sample was determined on the basis of a calibration curve generated from Cu^{II}-imidazole standards in N-ethylmorpholine buffer at pH 7.22 containing 50% glycerol (v/v). The concentration of Cu^{II} in each of the EPR standards was assayed by chelation with bathocuproine disulfonic acid (BC) and reduction with ascorbate.[25] The quantity of total copper as $[Cu(BC)_2]^{3-}$ was quantified at 483 nm (ε_{483} = 12500 M^{-1} cm^{-1}).[25] The 0, 25, 50, and 100 μM Cu^{II} standards contained 2.0 ± 1.0, 21 ± 1.0, 61 ± 0.4, and 119 ± 1.2 μM Cu^{II}, respectively.

Assessment of Aβ16 Damage Following Multiple Redox Cycles by HPLC

A 1.0 mL 0.10 mM solution of $A\beta16Cu^{II}$ was prepared as outlined above using a 1:1 Cu^{II}:Aβ16 stochiometry. Throughout the experiment aliquots were sampled from the main reaction vessel, and were analyzed by HPLC on a Waters DeltaPrep 60 equipped with an X-Terra C-18 reverse phase column (5 μm; 4.6 × 100 mm) using a gradient of 10-45% MeCN (0.1 % trifluoroacetic acid) in H_2O (0.1% trifluoroacetic acid) over 25 min. Following the initial analysis of the $A\beta16Cu^{II}$ solution, the sample was then reduced with 1.0 equivalent of ascorbate. After 19 hours the sample was reanalyzed by HPLC, rereduced with 1.0 equivalent of ascorbate, and then reanalyzed after 19 hours. The sample was then rereduced with an additional 1.0 equivalent of ascorbate and analyzed a final time after an additional 19 hours. In each case 50 μL of sample was added to 50 μL of a stock solution containing 0.100 mM of the peptide H_2N-GAATDAQ-COOH as an internal standard and then analyzed by HPLC. Samples were not stirred throughout the course of the experiment, but were agitated by wrist for ~15 sec. upon addition of ascorbate, and remained exposed to air throughout the experiment. All chromatograms were quantified using the software program PeakFit (SeaSolve Software, Inc.; Framingham, MA). The chromatograms displayed are baseline corrected.

EPR Spectroscopy

EPR spectra were collected on a Bruker EMX 6/1 spectrometer equipped with a microwave frequency meter and an Oxford Instruments ESR900 liquid He cryostat system. All spectra were collected with the following experimental parameters: microwave frequency = 9.38 GHz, microwave power = 0.5 mW, modulation amplitude = 10 G, time constant = 40.96 ms, conversion time = 40.96 ms, gain = 5×10^4, eight scans, temperature 20 K. Spectra of calibration standards were collected every run and a calibration curve to determine the Cu^{II} concentration was generated. The error associated with Cu^{II} concentrations determined using the calibration curve is estimated to be a maximum of 5-10 μM (about 10%) on the basis of comparison of spectra of the calibration standards collected on different days.

EPR samples for experiments with ascorbate were prepared in quartz EPR tubes capped with a tip-off manifold from Wilmad. Samples were degassed under inert atmosphere (dinitrogen

or argon) using 3 freeze-pump-thaw cycles on a vacuum line. Stock solutions of sodium ascorbate for EPR experiments were prepared by adding solid sodium ascorbate to MQ water that had been thoroughly degassed on the vacuum line prior to addition of the solid. Aliquots of sodium ascorbate were removed from the stock solution under a blanket of inert gas and injected into the EPR sample, which was maintained under an inert atmosphere during the process. The addition and mixing was complete in less than 2 min typically.

Air was introduced into the EPR samples by freezing them to 77K, evacuating the sample headspace on the vacuum line, and admitting air into the headspace. Subsequently, the sample was thawed and mixed by inversion of the tube and its contents several times.

XAS Data Measurement and Analysis

The copper-containing peptide solutions were injected into aluminum sample holders in between two windows made of Kapton tape (3M, cat. #1205; Minneapolis, MN) and quickly frozen in liquid nitrogen. The Aβ40Cu^{II} sample was prepared and handled at 0 °C to maintain the monomeric peptide state.[26] Data were then collected at the National Synchrotron Light Source (Brookhaven National Laboratories; Upton, NY) on beamlines X9b and X3b (ring operating conditions: 2.8 GeV; 200 – 305 mA). A focused Si(111) double monochrometer was used for energy selection along with a low-angle (4.5 mrad) Ni mirror for harmonic rejection. Energy calibrations were performed by recording a reference spectrum of Cu foil (first inflection point assigned to 8980.3 eV) simultaneously with the samples. All samples were maintained at 20 K throughout the data collection using a helium Displex cryostat. The spectra are reported as fluorescence data, which were recorded utilizing a 13-element Ge solid-state fluorescence detector (Canberra). Total count rates were maintained under 20 kHz per channel, and a deadtime correction of 3 μs was utilized (this had a negligible influence on the data). For XANES spectra the primary hutch aperture height was set to 0.4 mm to obtain the maximum resolution (theoretical maximum is ~0.9 eV), while the hutch aperture was set to 1 × 2 mm, and data were obtained in 10 eV steps in the pre-edge region (8779 – 8958 eV), 0.3 eV steps in the edge region (8959 – 9023 eV), and 2.0 eV steps in the near-edge region. For EXAFS spectra the primary hutch aperture was set to 0.8 mm, the hutch aperture was set to 1 × 8 mm, and data were obtained in 5.0 eV steps in the pre-edge region (8779 – 8958 eV), 0.5 eV steps in the edge region (8959 – 9023 eV), 2.0 eV steps in the near-edge region (9024 – 9278 eV), and 5.0 eV steps in the far-edge region (9279 eV – 14.0 k). The EXAFS spectra represent the averaged sum of 20 spectra, while the XANES spectra represent the averaged sum of 3 spectra. After every other scan the beam was moved to a different position on the sample to avoid potential radiation damage. All spectra were individually inspected prior to data averaging to insure that sample decomposition in the beam was not occurring.

Data analysis was performed as previously described using the XAS analysis package EXAFS123.[27,28] The only deviation is that the number of scatterers in the individual shells were initially left as free parameters, and then restrained to the nearest whole number. Single scatterer functions for Cu-N, Cu-O, and Cu-C interactions were constructed as previously described.[27,29] Multiple scattering (MS) pathways for the Cu-Im moiety were constructed by removal of the Cu-N single scattering interaction from 48 simulated reference spectra. These reference spectra were then used to construct the MS pathways in an analogous manner as before, where three refinable parameters are considered: the Cu-"N" distance (r(Im)), the in-plane angle (ϕ), and the out of place angle (θ; see Chart 1). For utilization of these MS pathways in the EXAFS analysis we restrained r(Im) to be equal to that of the single scatterer Cu-N distance, and then allowed the two angles to refine freely. Although data were collected to 14 k, data refinements were only performed out to k = 12.0 $Å^{-1}$ due to noise at higher values of k. Best fits to the experimental data were determined by selecting the model that gave both

chemically reasonable refinement parameters and the lowest value for the goodness of fit parameter:

$$\mathrm{GOF}=\mathrm{ave}[(\chi-\chi_{\mathrm{sim}})/\mathrm{esd}_{\mathrm{data}}](n_i/(n_i-n_p))^{1/2} \quad (1)$$

where n_i is the number of independent data points and n_p is the number of parameters used in the data simulations.

The bond valence sum (BVS) analysis[30] on all refined EXAFS models was applied according to:

$$s_i=\exp[(r_o-r)/0.37] \quad (2)$$

$$\mathrm{BVS}=\sum s_i \quad (3)$$

where r is the experimentally derived (EXAFS) bond length for ligand i and r_o is the reference bond-length. The values used for r_o include: $r_{Cu(II)N}$ = 1.751 Å; $r_{Cu(II)O}$ = 1.679 Å; and $r_{Cu(I)N}$ = 1.595 Å.

Results and Discussion

Aβ16Cu^{II} Cu K-edge XAS

The Cu K-edge XAS obtained for the Cu^{II} adduct of Aβ16 is depicted in Figure 1. The edge region is characterized by a weak transition at 8979.7(1) eV that corresponds to the parity forbidden Cu(1s → 3d) transition and a shoulder in the edge region at 8986.8(1) eV that corresponds to a Cu(1s → 4p + shakedown) transition.[31,32] The corresponding normal Cu(1s → 4p) transition is not resolvable from the edge.

The EXAFS region was best modeled with Cu^{II} contained in a square-planar coordination environment with N/O ligation (Table 1; Figure 1). These refinements yielded three N/O scatterers at 1.938(12) Å and a fourth N/O scatterer at 2.07(2) Å. As can be seen, the magnitude Fourier Transformed (FT) EXAFS shows strong outersphere scattering between r = 2 to 4 Å, which is characteristic of multiple scattering (MS) interactions between the Cu-center and rigid ligands (i.e. imidazole rings from histidine residues). Using a MS analysis we were able to determine that two of the three shorter N/O scatterers are imidazole scatterers. In addition to the distance parameter, the phase and amplitude functions utilized to refine the MS pathways also yielded the in (ϕ) and out (θ) of plane Cu-His angles (see Chart 1). The resulting angles are best refined to a θ = 8(3)° and a ϕ = 129(8)°. These are both consistent and reasonable for Cu-His ligation. We note that this represents the average of the two imidazole scatterers, and an analysis where the two imidazole scatterers were separated into different shells gave identical results. Addition of more or fewer imidazole functions to these refinements yielded either poorer fits to the data, unrealistic angles for the Cu-Im moiety, or instability in the data refinements. Attempts were made to identify a fifth longer ligand without success.

A bond valence sum (BVS) analysis was utilized to determine if these refinements make chemical sense.[30] In this empirical analysis the metal-ligand bond length derived from the EXAFS data is compared to a reference bond length, and a bond valence (s_i) is obtained.

Summing up the bond valences for all of the metal-ligand distances in the complex gives the BVS. The strength of the BVS analysis is that it yields the same value for all transition metal complexes of the same metal type and oxidation state (e.g. Cu^{II}) *irrespective of coordination number and ligand type*. In the most widely applied variant of the BVS analysis, the reference bond lengths are chosen such that the resulting BVS will equal the transition metal ion's oxidation state. Therefore, for Cu^{II} the BVS should ideally be equal to 2. A BVS analysis is extremely helpful in evaluating EXAFS data, where the number of scatterers is the least reliable parameter obtained, because models that only differ by the number of scatterers in the same shells can be readily compared and contrasted on the basis of the BVS to determine which is most likely.

When a BVS analysis is applied to the above EXAFS data (Cu^{II} ligated by two N-imidazole scatterers and two N or O ligands) we calculate a BVS ranging from: 2.05 for a $Cu^{II}(N^{Im})_2(O)_2$ coordination model, either 2.13 or 2.16 for a $Cu^{II}(N^{Im})_2(N)(O)$ coordination model (depending on the long vs. short ligand identity), and 2.23 for the $Cu^{II}(N^{Im})_2(N)_2$ coordination model. The three possible models above with both N and O ligands in the primary coordination sphere gives BVS values that are most consistent with Cu^{II}, while the coordination model with four nitrogen based ligands gives a BVS that is likely too large to be consistent with Cu^{II}. Increasing the coordination number to five causes the resulting BVS to range between 2.40 to 2.84 depending on the number of N or O ligands, which are far too high to be consistent with Cu^{II}. Therefore our XAS data are fully consistent with a four coordinate Cu^{II} center ligated by two N-imidazole scatterers and two N or O ligands.

On the basis of these data alone it is impossible to identify if the two non-imidazole ligands are nitrogen or oxygen donors. It is also impossible to determine the identity of the ligands. There is good evidence, however, that one of these ligands is an N-atom donor derived from the N-terminal amine nitrogen.[8,9,18] One consideration is whether the N-terminal amine group coordinates inter- or intramolecularly. In an intermolecular coordination mode, a Cu^{II} ion could be anchored to histidine residues in one peptide and bind the amino terminus from a second peptide. If each peptide binds one Cu^{II} ion and provides a ligand to another Cu^{II} ion via the amino terminus, a 1:1 Cu:peptide stoichiometry would result, but the molecular mass of the species would be twice that of a simple intramolecular AβCu complex. We performed gel filtration chromatography of $A\beta Cu^{II}$ to rule out this possibility (Figure S2) and find that the molecular weight of the $A\beta Cu^{II}$ species corresponds to a monomeric complex. In addition, the mass spectrometry results of Jiang et al. show that only a 1:1 complex is detected for $A\beta 40Cu^{II}$.[10] Although neither of these results rule out a small population (< ~1%) of dimer resulting from intermolecular copper-ligation, the vast majority is due exclusively to intramolecular copper-ligation.

We speculate that the other N/O atom donor is likely an O-atom of a carbonyl group, perhaps from a carbonyl group of the peptide backbone. We suggest this possibility because one of our Cu^{II}-N/O atom distances determined from the EXAFS refinements (2.07 Å) is close to the Cu^{II}-O atom carbonyl distances measured in crystallographically-characterized Cu^{II}-peptide complexes. Cu^{II} bound to a prion octarepeat peptide fragment has a Cu^{II} O-atom distance of 2.067 Å.[33] In that structure, Cu^{II} is coordinated to two backbone amides, one histidine, and a backbone carbonyl in the equatorial plane.[33] In addition, a 2.04 Å distance was reported for Cu^{II} coordinated to a carbonyl O-atom in the equatorial plane in a cylic bis-histidine peptide.[34] It should be noted that tyrosine has been ruled out as the O-atom donor ligand to Cu^{II} by numerous spectroscopic experiments.[9,11,14,18]

Our model for $A\beta 16Cu^{II}$ can be contrasted with a recently published model for $A\beta 40Cu^{II}$ by Morante and coworkers based on Cu K-edge XAS data.[35] Because the Cu^{II} coordinating residues are all found within the first 16 residues of the N-terminus of Aβ, Aβ16 is a good

model of Cu^{II} coordination to Aβ40.[8,9,36] In the previous EXAFS study the Cu^{II} ion was modeled in a five coordinate square pyramidal geometry ligated by: two His scatterers at 1.94 Å, one shorter His scatterer at 1.85 Å, a Tyr oxygen scatterer at 2.00 Å, and a water at 1.91 Å. In our view the data presented by Morante are of insufficient quality to reliably separate similar scatterers at those distances; because the quality of the data presented by Morante are sufficient for analysis only between $k = 3.5 – 10.5$, the spectral resolution of their EXAFS data is only $\Delta r > 0.22$ Å at best (calculated from $\Delta r = \pi/(2\Delta k)$). Even with a sophisticated MS analysis the reliable separation of the two different imidazole shells and the phenol shell would be both extremely difficult (if not impossible) and still yield statistically meaningless structural parameters given the quality of the data.

To discount changes in the microenvironment about the Cu-center induced by the differences in the length of the Aβ fragment in this *vs.* Morante's study, a reanalysis of the EXAFS data as presented in the manuscript of Stellato et al. was undertaken. This reanalysis yields structural parameters consistent with our refinements from above (see Supporting Information; Table S2, Figure S3). In fact, we find that because of the “penalty” imposed by the inclusion of additional refinement parameters in our error analysis, our 4-coordinate (2 imidazole/2 N or O scatterers) model actually affords a slight statistical improvement over their 5-coordinate model using Morante's data.

Our re-analysis of the Stellato et al. EXAFS data in-and-of itself obviously does not preclude a 5-coordinate model, but a BVS analysis of the structural models does. Using their original refinement[35] (and our 5-coordinate re-refinement of their data), we arrive at a BVS between 2.87 – 2.92, while 4-coordinate refinements of these data yield a BVS that ranges between 2.02 – 2.31 depending on the CuN_2O_2 or CuN_4 models. This result means that a five coordinate formulation for Aβ16Cu^{II} or Aβ40Cu^{II} is most likely incorrect. The issues with the original refinement of the low resolution data collected by Stellato et al.,[35] our re-refinement of their data indicating that a 5-coordinate geometry is untenable, and refinement of our own higher resolution data, makes us strongly favor a 4-coordinate Cu^{II} model with two imidazole scatterers over a 5-coordinate model for the Aβ-Cu^{II} adduct.

A very recent combined DFT/Cu K-edge XAS study by Streltsov *et. al.*[16] on AβCu^{II} and several AβCu^{II} derivatives was performed at a similar resolution to our study (in fact our data are virtually superimposable), and at a considerably higher resolution than the study of Stellato *et. al.*[35] That study arrived at a different Cu-coordination environment than either Stellato or us; Streltsov *et. al.* propose a six coordinate structure with Cu^{II} ligation provided by three His imidazole nitrogens, both carboxylate oxygens from either Glu11 or Asp1, and another oxygen from a water molecule. Although the fit to the EXAFS data appears to be statistically valid there are two reasons why the chemical interpretation of Streltsov *et. al.* is questionable. There is general agreement from other spectroscopic data and recent theoretical work that Cu^{II} binds in a 4-coordinate square planar coordination environment within Aβ.[8,9,18,19] Several of the spectroscopic methods applied to the AβCu^{II} complex cannot directly detect axial ligands, which means that a 5 or 6-coordinate Cu^{II} coordination geometry cannot be definitively ruled out, but the BVS produced by the Streltsov model is 2.64, which is considerably too high for Cu^{II}. Our BVS analysis is therefore key to affirming the general consensus from other spectroscopic and theoretical work that Cu^{II} is bound to Aβ in a 4-coordinate geometry.

Aβ16Cu^{I} Cu K-edge XAS

The Cu K-edge XAS of ascorbate reduced Aβ16Cu^{I} is presented in Figure 2; similar data were obtained for Aβ40Cu^{I} (Supporting Information; Figure S4) indicating identical coordination modes for Aβ40Cu^{I} and Aβ16Cu^{I}. A comparison of the edge regions of Aβ16Cu^{II} (Figure 1) *vs.* Aβ16Cu^{I} shows that upon reduction the edge energy decreases by 4.2(6) eV, which is consistent with the reduction of Cu^{II} to Cu^{I}. Consistent with our results, Streltsov et al. report

a >5 eV shift in edge energy upon reduction of Aβ16Cu^{II} with ascorbate.[15] The XANES region of the XAS for Aβ16Cu^{I} displays an intense pre-edge feature at 8984.1(2) eV, which is assigned as the Cu(1s → 4p) transition.[31] For Cu^{I} this feature is highly dependent on coordination geometry about the Cu^{I} center. The position and intensity of the Cu(1s → 4p) transition observed for Aβ(16)Cu^{I} is consistent with either a two-coordinate linear geometry about Cu^{I}, or possibly a three coordinate T-shaped geometry.[31,37] However, as will be shown, the reactivity of AβCu^{I} is most consistent with a two-coordinate linear geometry.

A best fit to the EXAFS yielded a two coordinate geometry with two imidazole ligands coordinated to Cu^{I} at 1.877(2) Å (θ = 2(2)°; ϕ = 130(11)°; Scheme 1). Refinement of the data splitting the two imidazole scatters into different shells resulted in similar bond angles for the imidazole ligands (Figure S5). Attempts were made to solve for a three coordinate ligation environment for Aβ16Cu^{I}.[16] In all cases a T-shaped geometry could not be refined: the shell containing a third imidazole scatterer was always placed at distance nearly identical to the shell containing the other two imidazole scatterers. A BVS analysis of the two refinements yields a BVS = 0.94 for the two coordinate complex and 1.42 for the three coordinate complex. We therefore favor a linear two coordinate Cu^{I} coordination environment for Aβ16Cu^{I} on the basis of the Cu K-edge XAS coupled with the BVS analysis.

AβCu^{II}/AβCu^{I} EPR spectroscopy

Spectra for both Aβ16Cu^{II} and Aβ40Cu^{II} samples before and after the addition of ascorbate are shown in Figure 3. After the addition of ascorbate, the EPR signal decreases due to the disappearance of the AβCu^{II} complex, indicating the formation of the d^{10}, EPR-silent AβCu^{I} complex. Maiti et al. were the first to report that the reduction of Aβ16Cu^{II} and O_2-reoxidation of Aβ16Cu^{I} are completely reversible as observed by fluorescence spectroscopy.[14] This observation is inconsistent with our EPR spectroscopic data.

For the Aβ16Cu^{II} sample, spectral integration indicates that approximately 90% of the initial AβCu^{II} content is recovered in a sample treated with 1.2 equivalents of ascorbate under inert atmosphere followed by 19 h of air exposure. We note that if an ascorbate-treated sample is immediately treated with excess Ir(IV), the initial AβCu^{II} signal hyperfine intensity recovers entirely (Figure S6). In this case, spectral integration to quantify the AβCu^{II} concentration is not reliable because of a contribution from the broad EPR signal of unreacted Ir^{IV}. For Aβ40Cu^{II}, a similar pattern of sluggish O_2 reactivity was observed even under conditions where only 0.5 equiv of ascorbate was added (Figure 3B). The Cu^{II} concentrations for the 13 and 28 min time points for the AβCu^{II} + ascorbate reaction are the same within error (Figure 3B, inset), which indicates that the reduction reaction is complete after this time. After 19 h in air, the Cu^{II} concentration recovers to approximately 80% of its initial value. A matched sample treated with a 2-fold excess of ascorbate recovered only 60% of the initial Cu^{II} signal after 3 d in air (Figure S7). Finally, Aβ40Cu^{II} was reduced with a 4-fold excess of ascorbate in air-saturated solution (Figure S8). The EPR signal from Aβ40Cu^{II} decreased to about 15% of the initial signal. Like the sample treated with excess ascorbate under Ar, only about 60% of the initial Cu^{II} intensity is recovered in this sample after extended incubation (5 d) at room temperature.

In all of the samples prepared anaerobically and then exposed to oxygen, the Cu^{II} spectral shapes are the same pre- and post-ascorbate addition, suggesting that Cu^{II} is bound in its original coordination site after its reduction and reoxidation. The experiment performed in air, however, has slight differences in the spectral shape pre and post-ascorbate addition (Figure S8, inset). The post-ascorbate addition spectrum appears to contain contributions from two different Cu^{II} species. The appearance of a new Cu^{II} signal could be due to protein modification from carbonate radicals that are generated upon redox cycling of Cu.[38,39] Under conditions where the sample was degassed, all dissolved gases were removed prior to admitting air. Thus, samples made in air-saturated buffer contain more CO_2 than samples that were degassed.

Addition of carbonate radicals to proteins does not fragment the protein,[39] but instead introduces modifications. Such modifications might change the protein structure and/or metal binding sites leading to our observation of two types of Cu^{II} EPR signals in aerobic samples treated with ascorbate.

The fluorescence data of Miati et al. indicate that the Aβ16Cu^{II} complex is completely regenerated upon exposure of the AβCu^{I} complex to O_2.[14] In contrast, our EPR spectroscopic results indicate that the initial full concentration of AβCu^{II} complex is not regenerated upon oxidation of AβCu^{I}. As EPR spectroscopy is a direct indicator of the Cu^{II} coordination environment, whereas tyrosine fluorescence quenching is an indirect measure of Aβ–Cu^{II} coordination, our more sensitive data strongly suggest the loss of Cu^{II} binding affinity toward Aβ.

There are several possible explanations for why an EPR signal from AβCu^{II} does not reappear entirely upon air exposure of anaerobic samples treated with ascorbate. One possibility is that some fraction of Cu^{II} is released from the peptide because of oxidative decomposition of the peptide (*vide infra*). This released Cu^{II} will bind to phosphate buffer to make an antiferromagnetically-coupled Cu^{II} polymer that is EPR silent. Another possibility is that a stable Cu^{I} compound forms or some other type of copper cluster that is EPR silent. Our HPLC results (*vide infra*) are consistent with oxidative damage of the peptide.

The reaction of AβCu^{II} with a large excess of reductant has been reported to produce hydrogen peroxide, hydroxyl radicals, and tyrosine radicals.[3,13,40-42] Tyrosyl radical, in particular, has been proposed as an intermediate in ROS generation by the AβCu complex.[40,42,43] Under our conditions, AβCu^{II} with ascorbate does not produce a detectable amount of tyrosine radical, a species that is easily identifiable by low-temperature EPR spectroscopy.[44] This result indicates that this radical does not reach a steady-state concentration above our detection limit. Barnham et al. proposed catalytic tyrosine radical formation as part of the ROS-generating mechanism for AβCu,[42] which contradicts peptide oxidation detected by mass spectrometry showing that histidine oxidation appears prior to tyrosine oxidation and crosslinking reactions.[45,46] Thus, it remains unclear whether tyrosine radical formation precedes, is concerted with, or follows hydrogen peroxide/hydroxyl radical production.

Assessment of Oxidative Damage of Aβ16 Following Multiple Cu Redox Cycles

Our EPR results clearly show that regeneration of AβCu^{II} is not quantitative following redox-cycling, which may be indicative of peptide damage to the copper ligating residues of Aβ or other processes that change the physiochemical nature of Aβ16, as has previously been observed.[47] We probed the supposition that peptide damage may be responsible for the non-quantitative regeneration of AβCu^{II} by following multiple redox cycles using HPLC (Figure 4). Prior to reduction of Aβ16Cu^{II} by ascorbate the metallopeptide shows one distinct peak in the chromatogram. Following reduction of Aβ16Cu^{II} with one equivalent of ascorbate and 19 hours of air oxidation, three new peaks have appeared in the chromatogram, and the amount of Aβ16Cu^{II} has decreased by 33% of its original concentration compared to a peptide standard. After a second redox cycling under identical conditions more Aβ16Cu^{II} has been lost (56% of its original concentration), the additional peaks have increased in intensity, a fourth peak has grown in, and there is a significant amount of material that comes off the column only towards the end of the HPLC run (and in the column wash), which is indicative of peptide oligomerization. After a third and final redox cycling, the amount of Aβ16Cu^{II} remaining in solution is 39% of its original concentration, while the amount of material coming off at the end of the run has increased a significant amount indicating increased peptide aggregate formation, and a fifth broad peak between 11-13 min, has appeared in the chromatogram.

The HPLC redox cycling results confirm the EPR results from above: damage to Aβ16Cu^{II} is occurring following multiple redox cycles. Control HPLC and GPC studies demonstrate that Aβ16Cu^{II} does not undergo significant damage or oligimerization if a reductant is not added to solution (Figures S2 and S9). This strongly suggests that redox cycling is accelerating the deterioration of monomeric Aβ16Cu^{II}. It is likely that similar oxidative damage to Aβ16 is occurring here as was previously observed by Schöneich and Williams, who observed predominant oxidation of His13 and His14.[47] We are currently in the process of identifying the Aβ modification sites and identity of the oxidized products to confirm this supposition.

These HPLC results indicate that slightly more oxidative damage to Aβ16Cu^{II} is occurring during redox cycling than indicated by EPR, as there is a significantly larger decrease in soluble monomeric Aβ16Cu^{II} observed by HPLC than EPR. There are at least three possible explanations for this observation. The first is that one (or more) of the modified Aβ16 products is capable of coordinating Cu^{II} in a ligand environment nearly identical to that of unmodified Aβ16. Another explanation is that redox cycling produces soluble, crosslinked Aβ16Cu^{II} oligomers, which are spectroscopically similar by EPR, but distinguishable by HPLC. The third explanation is that the EPR samples contained less oxygen than the HPLC samples. The buffer was the same for both sets of samples so the O_2 solubility in the solvent system is the same. However, following air exposure, EPR samples were sealed and not reopened, which means that no additional air (and, therefore, O_2) was introduced. We calculate that there are 14.7 μmol of O_2 in the headspace of the EPR tube compared to 0.01 μmol of Cu in the sample, which represents a 1500-fold excess of O_2 over Cu. Nevertheless, the HPLC samples were prepared and handled in air so that the amount of air in the samples could be higher than in the EPR samples.

Summary and Biological Implications

In this study we have shown that Cu^{II} adducts of Aβ can readily undergo reduction by the biologically relevant reductant ascorbate.[48] By XAS we have shown that upon reduction of Aβ16Cu^{II} and Aβ40Cu^{II} with ascorbate linear His_2-Cu^{I} adducts are formed (Scheme 1). Our XAS analysis is therefore consistent with the observed O_2 reactivity displayed by Aβ16Cu^{I} and Aβ40Cu^{I}. Following reduction of AβCu^{II} with stoichiometric amounts of ascorbate, solutions of Aβ16Cu^{I} or Aβ40Cu^{I} are not highly sensitive to O_2, requiring hours to undergo conversion from Cu^{I} to Cu^{II}. Similarly, solutions of two coordinate Cu^{I} complexes are not susceptible to oxidation by dioxygen.[37,49] In contrast, three coordinate Cu^{I} centers are highly reactive towards dioxygen, typically undergoing oxidation to Cu^{II} instantaneously upon exposure to dioxygen.[37,50] Therefore, the dioxygen reactivity of Aβ16Cu^{I} is consistent with the our XAS analysis.

A recent study by Karlin and coworkers is also consistent with our formulation of a linear diimidazole Cu^{I} ligation scheme for Aβ16Cu^{I}.[37] In that study, a series of His-His dipeptides coordinated to Cu^{I} formed linear two coordinate copper centers with Cu-imidazole bond lengths ranging from 1.863 – 1.876 Å. These two-coordinate Cu^{I}-dipeptides were not prone to oxidation by O_2. However, upon the addition of a third imidazole-based ligand to the Cu^{I}-dipeptides the rapid oxidation of Cu^{I} to Cu^{II} was noted in that study. Therefore, the O_2 reactivity of Aβ16Cu^{I} and Aβ40Cu^{II} are both most consistent with a linear diimidazole-Cu^{I} ligation scheme.

In addition to providing experimental precedence in support of our coordination mode for Aβ16Cu^{I} and Aβ40Cu^{I}, Karlin's study hints at the identity of the two His residues ligated to Cu^{I} in these metallopeptides. The copper-binding domain of Aβ contains two adjacent His residues at positions 13 and 14, making it reasonable to speculate that His13 and His14 are the residues involved in Cu^{I} coordination in Aβ. Computational studies by both us and Karlin

indicate that the linear Cu^{I} bis-His motif is not strained, and we in-fact arrive at nearly identical structural parameters for the $[Cu^{I}(His)_2]^{+}$ metallopeptide using high-level double hybrid DFT methods as we determined by EXAFS (Figure S10, Table S3). Indeed, mass spectrometry of oxidative damage products generated upon reduction of $A\beta Cu^{II}$ with ascorbate indicates that His13 and His14 are preferentially oxidized at short reaction times,[46] not His6, suggesting His13 and His14 are the sidechains bound to Cu^{I}. Although it is possible that one of these two histidines is damaged because of proximity to copper and not direct ligation, it is difficult to explain why His6 is not damaged if it is one of the two histidine ligands to copper.

Another finding of this study that has broad implications for our understanding of the etiology of the AβCu complex is the oxidative damage of the reduced metallopeptides following oxidation by O_2. It has been shown that $A\beta Cu^{II}$ in the presence of reductants generates ROS.[13,51] We ascribe incomplete recovery of the $A\beta Cu^{II}$ EPR signal to ROS-induced peptide damage, in particular histidine oxidation,[12,40,47,52] that precludes Cu^{II} binding in the native coordination site. Our HPLC results also indicate that multiple redox cycling produces significantly more Aβ damage following each cycle; there is a non-linear increase in Aβ damage following each redox cycle. This leads us to predict that when aerobic solutions of $A\beta Cu^{II}$ are redox-cycled via addition of excess ascorbate, an evolving and heterogeneous mixture of Cu species is created: copper ions bound to modified and unmodified peptide and copper ions not bound to the peptide are all present.

It has been shown that addition of an exogenous chelator to solutions of $A\beta Cu^{II}$ treated with ascorbate retards hydrogen peroxide production.[53] This result is entirely consistent with the fact that chelated Cu^{II} is reduced more slowly by ascorbate than "free" Cu^{II} ion.[54] Such heterogeneity of the $A\beta/Cu^{II}$/reductant reaction mixture and details of the rate constant/mechanism differences between bound and unbound copper have not been considered carefully previously. In our view, these critical issues call into question measurements of the rates of hydrogen peroxide and/or hydroxyl radical production by $A\beta Cu^{II}$, which have assumed a single species (Cu-ligated Aβ) is responsible for ROS formation.[10,13] Both Cu^{II} that is not bound to peptide and copper-ligated Aβ may be producing ROS, but we believe Cu^{II} released from oxidatively-modified Aβ is the principal ROS generator in this system.

Together, these findings suggest several hypotheses concerning Aβ and its role in neurodegeneration. First, under redox-cycling conditions, oxidative damage to Aβ inhibits its ability to bind Cu, and thus will promote oxidative stress in neuronal tissue. Also, these data point towards the supposition that copper-induced ROS generation mediates Aβ aggregation, as has been previously suggested.[40,55] Upon multiple rounds of redox cycling of $A\beta16Cu^{II}$, it appears that significant Aβ16 aggregation, perhaps via covalent crosslinking, occurs. Oxidative modification of Aβ increases its propensity to aggregate, which has been hypothesized to increase Aβ oligomer formation and/or plaque deposition in AD.[40,42,56]

Finally, we propose that AβCu may be neuroprotective[57] if it forms a Cu^{I} complex rather than a Cu^{II} complex *in vivo*. We come to the conclusion that AβCu might be neuroprotective based on our EXAFS results, which are consistent with the O_2-stable linear Cu^{I} coordination geometry, and a thermodynamic square scheme (Scheme 2). This scheme predicts a higher affinity of Aβ for Cu^{I} than for Cu^{II} because the midpoint potential of $A\beta Cu^{II}/A\beta Cu^{I}$ is higher (0.28 V[10] vs. NHE) than that of free Cu^{II}/Cu^{I} (0.158 V vs. NHE).[58] Note that the magnitude of the affinity of Aβ for Cu^{II} has no effect on the *relative* affinities of Aβ for Cu^{I} vs. Cu^{II}. Our assumption that the "free" Cu^{II}/Cu^{I} potential is lower than that of the $A\beta Cu^{II}/A\beta Cu^{I}$ complex is supported by electrochemistry experiments that showed that Cu^{II} in buffer is reduced at a lower potential than $A\beta Cu^{II}/A\beta Cu^{I}$ in the same buffer.[10] If Aβ has a higher affinity for Cu^{I} than Cu^{II} and the $A\beta Cu^{I}$ complex is sluggish to react with O_2, damage from Cu ions will be abrogated in the presence of Aβ compared to Cu^{II}/Cu^{I} that is not bound to peptide. The redox-

cycling of AβCu depends on the concentrations of ascorbate and O_2 in vivo. Extracellular fluid that surrounds mammalian neurons, and is in equilibrium with cerebral spinal fluid (CSF), contains 200 – 400 μM ascorbate.[48] The pO_2 of CSF has been measured to be 31-51 mm Hg by invasive methods.[59] More recently, values obtained using fluid-attenuated inversion recovery (FLAIR) magnetic resonance imaging on humans are 54 ± 18 (lateral ventricles), 67 ± 1 (cisterna magna), 106 ± 42 (cortical sulci), and 130 ± 49 mm Hg (third ventrical), which gives an average of about 90 mm Hg in CSF.[60] For comparison, the pO_2 in the trachea is about 150 mm Hg. Thus, the concentration of O_2 in CSF is about 2-fold lower than in air-saturated solutions at 37 °C. Although our experiments were performed at room temperature instead of 37 °C and, therefore, the rates are different from those at 37 °C, we find that the $A\beta40Cu^{II}$ species can be reduced to $A\beta40Cu^{I}$ in an environment containing substantially more O_2 (air-saturated buffer) than is present in CSF. Although speculative, our idea that $A\beta Cu^{I}$ is the dominant species in vivo is consistent with our findings and represents a neuroprotective mechanism for AβCu that has not been proposed previously.

Supplementary Material

Refer to Web version on PubMed Central for supplementary material.

Acknowledgments

Funded by Alzheimer's Association Grant IIRG-07-5821 (V.A.S.) and NIH grant number P20 RR-016464 from the INBRE Program of the National Center for Research Resources, (J.S.) Use of the National Synchrotron Light Source, Brookhaven National Laboratory, was supported by the U.S. Department of Energy, Office of Science, Office of Basic Energy Sciences, under Contract No. DE-AC02-98CH10886.

References

1. Ferri CP, Prince M, Brayne C, Brodaty H, Fratiglioni L, Ganguli M, Hall K, Hasegawa K, Hendrie H, Huang Y, Jorm A, Mathers C, Menezes PR, Rimmer E, Scazufca M. Lancet 2005;366:2112. [PubMed: 16360788]
2. Castellani RJ, Lee HG, Zhu X, Perry G, Smith MA. J Neuropathol Exp Neurol 2008;67:523. [PubMed: 18520771] Sergeant N, Bretteville A, Hamdane M, Caillet-Boudin ML, Grognet P, Bombois S, Blum D, Delacourte A, Pasquier F, Vanmechelen E, Schraen-Maschke S, Buee L. Expert Rev Proteomics 2008;5:207. [PubMed: 18466052] Cechetto DF, Hachinski V, Whitehead SN. Expert Rev Neurother 2008;8:743. [PubMed: 18457531] Xia W. Curr Alzheimer Res 2008;5:172. [PubMed: 18393802] Windisch M, Wolf H, Hutter-Paier B, Wronski R. Neurodegener Dis 2008;5:218. [PubMed: 18322395] Luheshi LM, Crowther DC, Dobson CM. Curr Opin Chem Biol 2008;12:25. [PubMed: 18295611] Shi Q, Gibson GE. Alzheimer Dis Assoc Disord 2007;21:276. [PubMed: 18090434] Skovronsky DM, Lee VM, Trojanowski JQ. Annu Rev Pathol 2006;1:151. [PubMed: 18039111] Irvine GB, El-Agnaf OM, Shankar GM, Walsh DM. Mol Med 2008;14:451. [PubMed: 18368143] Selkoe DJ. Behav Brain Res 2008;192:106. [PubMed: 18359102]
3. Green KN, Smith IF, Laferla FM. Subcell Biochem 2007;45:507. [PubMed: 18193650]
4. Zhu X, Su B, Wang X, Smith MA, Perry G. Cell Mol Life Sci 2007;64:2202. [PubMed: 17605000]
5. Dong J, Atwood CG, Anderson VE, Siedlak SL, Smith MA, Perry G, Carey PR. Biochemistry 2003;42:2768. [PubMed: 12627941] Beauchemin D, Kisilevsky R. Anal Chem 1998;70:1026. [PubMed: 9511476] Miller LM, Wang Q, Telivala TP, Smith RJ, Lanzirotti A, Miklossy J. J Struct Biol 2006;155:30. [PubMed: 16325427]
6. Adlard PA, Bush AI, Adman ET. J Alzheimers Dis 2006;10:145. [PubMed: 17119284]
7. Karr JW, Szalai VA. Biochemistry 2008;47:5006. [PubMed: 18393444] Kowalik-Jankowska T, Dolejsz-Ruta M, Wisniewska K, Lankiewicz L. J Inorg Biochem 2001;86:535. [PubMed: 11566325] Ma QF, Hu J, Wu WH, Liu HD, Du JT, Fu Y, Wu YW, Lei P, Zhao YF, Li YM. Biopolymers 2006;83:20. [PubMed: 16615111] Danielsson J, Pierattelli R, Banci L, Graslund A. FEBS Journal 2007;274:46. [PubMed: 17222176] Lim KH, Kim YK, Chang YT. Biochemistry 2007;46:13523. [PubMed: 17973493] Hou L, Zagorski MG. J Am Chem Soc 2006;128:9260. [PubMed: 16848423]

8. Syme CD, Nadal RC, Rigby SEJ, Viles JH. J Biol Chem 2004;279:18169. [PubMed: 14978032]
9. Kowalik-Jankowska T, Ruta M, Wisniewska K, Lankiewicz L. J Inorg Biochem 2003;95:270. [PubMed: 12818797]
10. Jiang D, Men L, Wang J, Zhang Y, Chickenyen S, Wang Y, Zhou F. Biochemistry 2007;46:9270. [PubMed: 17636872]
11. Guilloreau L, Damian L, Coppel Y, Mazarguil H, Winterhalter M, Faller P. J Biol Inorg Chem 2006;11:1024. [PubMed: 16924555]
12. Kowalik-Jankowska T, Ruta M, Wisniewska K, Lankiewicz L, Dyba M. J Inorg Biochem 2004;98:940. [PubMed: 15149800]
13. Guilloreau L, Combalbert S, Sournia-Saquet A, Mazarguil H, Faller P. Chembiochem 2007;8:1317. [PubMed: 17577900]
14. Maiti NC, Jiang D, Wain AJ, Patel S, Dinh KL, Zhou F. J Phys Chem B 2008;112:8406. [PubMed: 18570397]
15. Streltsov VA, Varghese JN. ChemComm 2008;27:3169.
16. Raffa DF, Rickard GA, Rauk A. J Biol Inorg Chem 2007;12:147. [PubMed: 17013614]
17. Streltsov VA, SJ JT, Epa VC, Barnham KJ, Masters CL, Varghese JN. Biophys J. 2008 Epub ahead of print. 10.1529/biophysj.108.134429
18. Karr JW, Akintoye H, Kaupp LJ, Szalai VA. Biochemistry 2005;44:5478. [PubMed: 15807541]
19. Mantri Y, Fioroni M, Baik MH. J Biol Inorg Chem. 2008
20. Nakamura M, Shishido N, Nunomura A, Smith MA, Perry G, Hayashi Y, Nakayama K, Hayashi T. Biochemistry 2007;46:12737. [PubMed: 17929832]
21. Karr JW, Kaupp LJ, Szalai VA. J Am Chem Soc 2004;126:13534. [PubMed: 15479110]
22. Stine WB Jr, Dahlgren KN, Krafft GA, LaDu MJ. J Biol Chem 2003;278:11612. [PubMed: 12499373]
23. Miura T, Suzuki K, Kohata N, Takeuchi H. Biochemistry 2000;39:7024. [PubMed: 10841784]
24. Karr JW, Szalai VA. J Am Chem Soc. 2007
25. Moffett J, Zika RG, Petasne RG. Anal Chim Acta 1985;175:171.
26. Hou L, Shao H, Zhang Y, Li H, Menon NK, Neuhaus EB, Brewer JM, Byeon IJ, Ray DG, Vitek MP, Iwashita T, Makula RA, Przybyla AB, Zagorski MG. J Am Chem Soc 2004;126:1992. [PubMed: 14971932]
27. Shearer J, Soh P. Inorg Chem 2007;46:710. [PubMed: 17257012]
28. Scarrow, RC. Haverford College; Haverford, PA: 2005. www.Haverford.edu/chem./Scarrow/EXAFS123/ ed
29. Scarrow RC, S SB, Ellison JJ, Shoner SC, Kovacs JA, Cummings JG, Nelson MJ. J Am Chem Soc 1998;120:9237.Scarrow RC, Brennan BA, Cummings JG, Jin H, Duong DJ, Kindt JT, Nelson MJ. Biochemistry 1996;35:1078.
30. Brown ID, Altermatt D. Acta Crystallogr, Sect B 1985;41:244.Thorp HH. Inorg Chem 1992;31:1585.
31. Kau LS, Spira-Solomon DJ, Penner-Hahn JE, Hodgson KO, Solomon EI. J Am Chem Soc 1987;109:6433.
32. DuBois JL, Mukherjee P, Stack TDP, Hedman B, Solomon EI, Hodgson KO. J Am Chem Soc 2000;122:5775.
33. Burns CS, Aronoff-Spencer E, Dunham CM, Lario P, Avdievich NI, Antholine WE, Olmstead MM, Vrielink A, Gerfen GJ, Peisach J, Scott WG, Millhauser GL. Biochemistry 2002;41:3991. [PubMed: 11900542]
34. Kojima Y, Hirotsu K, Matsumoto K. Bull Chem Soc Japan 1977;50:3222.
35. Stellato F, Menestrina G, Serra MD, Potrich C, Tomazzolli R, Meyer-Klaucke W, Morante S. Eur Biophys J 2006:340. [PubMed: 16404590]
36. Curtain CC, Ali F, Volitakis I, Cherny RA, Norton RS, Beyreuther K, Barrow CJ, Masters CL, Bush AI, Barnham KJ. J Biol Chem 2001;276:20466. [PubMed: 11274207]
37. Himes RA, Park GY, Barry AN, Blackburn NJ, Karlin KD. J Am Chem Soc 2007;129:5352. [PubMed: 17411054]
38. Ramirez DC, Mejiba SE, Mason RP. J Biol Chem 2005;280:27402. [PubMed: 15905164]
39. Ramirez DC, Gomez-Mejiba SE, Corbett JT, Deterding LJ, Tomer KB, Mason R. Biochem J. 2008

40. Atwood CS, Perry G, Zeng H, Kato Y, Jones WD, Ling KQ, Huang X, Moir RD, Wang D, Sayre LM, Smith MA, Chen SG, Bush AI. Biochemistry 2004;43:560. [PubMed: 14717612]
41. Haeffner F, Smith D, Barnham K, Bush A. J Inorg Biochem 2005;99:2403. [PubMed: 16271394]
42. Barnham KJ, Haeffner F, Ciccotosto GD, Curtain CC, Tew D, Mavros C, Beyreuther K, Carrington D, Masters CL, Cherny RA, Cappai R, Bush AI. Faseb J 2004;18:1427. [PubMed: 15231727]
43. Tickler AK, Smith DG, Ciccotosto GD, Tew DJ, Curtain CC, Carrington D, Masters CL, Bush AI, Cherny RA, Cappai R, Wade JD, Barnham KJ. J Biol Chem 2005;280:13355. [PubMed: 15668252]
44. Szalai VA, Brudvig GW. Biochemistry 1996;35:15080. [PubMed: 8942675] Szalai VA, Brudvig GW. Biochemistry 1996;35:1946. [PubMed: 8639678] Szalai VA, Kühne H, Lakshmi KV, Brudvig GW. Biochemistry 1998;37:13594. [PubMed: 9753446] Stubbe J, van der Donk WA. Chem Rev 1998;98:705. [PubMed: 11848913]
45. Schoneich C. Ann N Y Acad Sci 2004;1012:164. [PubMed: 15105263]
46. Pogocki D, Schoneich C. Chem Res Toxicol 2002;15:408. [PubMed: 11896689]
47. Schoneich C, Williams TD. Chem Res Toxicol 2002;15:717. [PubMed: 12018994]
48. Rice ME. Trends Neurosci 2000;23:209. [PubMed: 10782126]
49. Sorrell TN, Jameson DL. J Am Chem Soc 1983;105:6013.Sanyal I, Strange RW, Blackburn NJ, Karlin KD. J Am Chem Soc 1991;113:4692.Sanyal I, Strange RW, Blackburn NJ, Karlin KD. J Am Chem Soc 1993;115:11259.
50. Lewis EA, Tolman WB. Chem Rev 2004;104:1047. [PubMed: 14871149]
51. Huang X, et al. J Biol Chem 1999;274:37111. [PubMed: 10601271]
52. Lim J, Vachet RW. Anal Chem 2003;75:1164. [PubMed: 12641237]
53. Deraeve C, Pitie M, Meunier B. J Inorg Biochem 2006;100:2117. [PubMed: 17011628]
54. Taqui Khan MM, Martell AE. J Am Chem Soc 1967;89:7104. [PubMed: 6064355] Taqui Khan MM, Martell AE. J Am Chem Soc 1967;89:4176. [PubMed: 6045609]
55. Smith DG, Cappai R, Barnham KJ. Biochim Biophys Acta. 2007
56. Yoburn JC, Tian W, Brower JO, Nowick JS, Glabe CG, Van Vranken DL. Chem Res Toxicol 2003;16:531. [PubMed: 12703970] Smith DP, Ciccotosto GD, Tew DJ, Fodero-Tavoletti MT, Johanssen T, Masters CL, Barnham KJ, Cappai R. Biochemistry 2007;46:2881. [PubMed: 17297919]
57. Zou K, Gong JS, Yanagisawa K, Michikawa M. J Neurosci 2002;22:4833. [PubMed: 12077180]
58. Weast, RC., editor. Handbook of Chemistry & Physics. 51st. The Chemical Rubber Company; Cleveland, OH: 1970.
59. Jarnum S, Lorenzen I, Skinhoj E. Neurology 1964;14:703. [PubMed: 14206560] Ganshirt H. Wien Med Wochenschr 1966;116:953. [PubMed: 5992463]
60. Zaharchuk G, Martin AJ, Rosenthal G, Manley GT, Dillon WP. Magn Reson Med 2005;54:113. [PubMed: 15968660] Zaharchuk G, Busse RF, Rosenthal G, Manley GT, Dillon WP. Proc Intl Soc Mag Reson Med 2005;13:66.

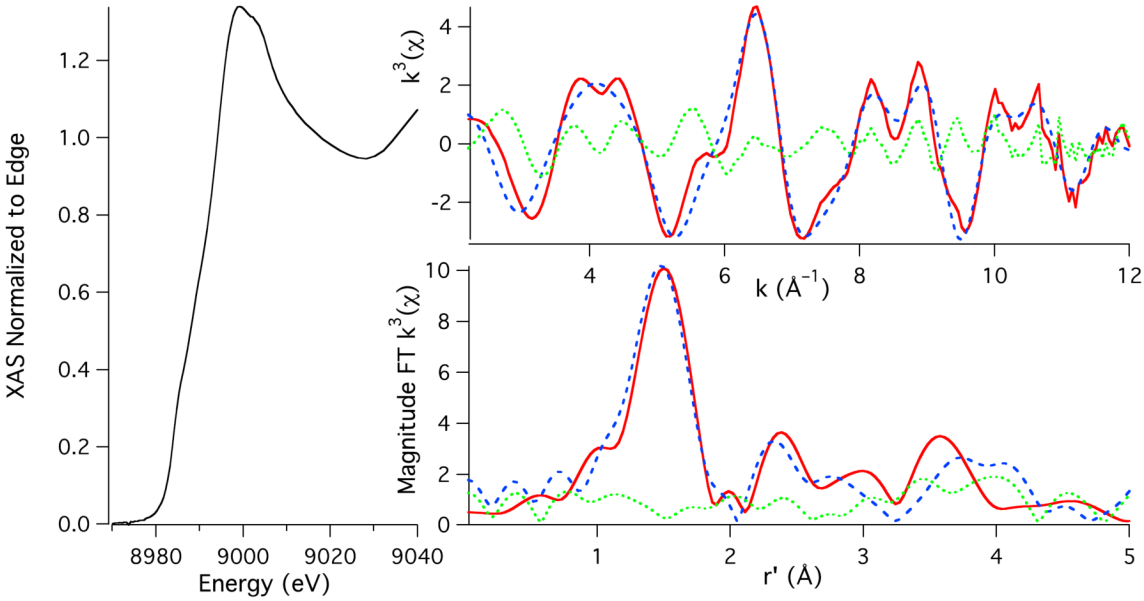

Figure 1.

Cu K-edge XAS of Aβ16Cu^{II}. The left portion of the figure depicts the XANES region of the XAS. The bottom and top right spectra depict the magnitude FT $k^3(\chi)$ and $k^3(\chi)$, respectively. The experimental data are given as the red spectra, the simulations to the data are given as the dashed blue spectra, and the difference between the experimental and simulations are given as the dotted green spectra.

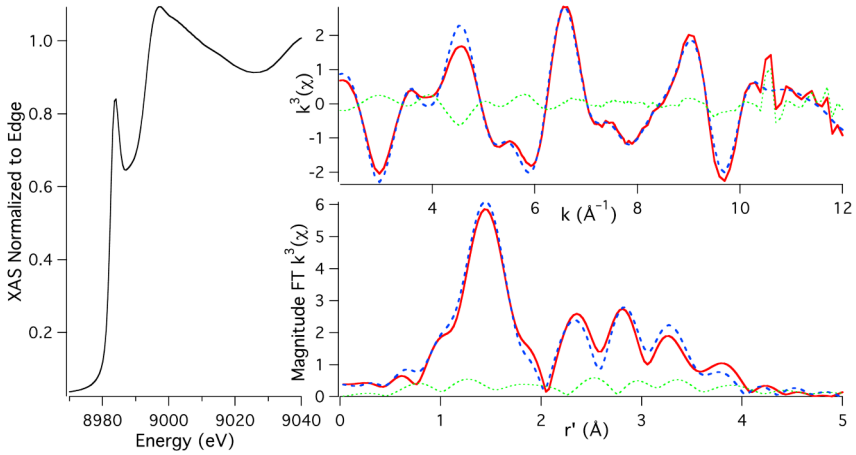

Figure 2.

Cu K-edge XAS of Aβ16Cu^{I}. The left portion of the figure depicts the XANES region of the XAS. The bottom and top right spectra depict the magnitude FT $k^3(\chi)$ and $k^3(\chi)$, respectively. The experimental data are given as the red spectra, the simulations to the data are given as the dashed blue spectra, and the difference between the experimental and simulations are given as the dotted green spectra.

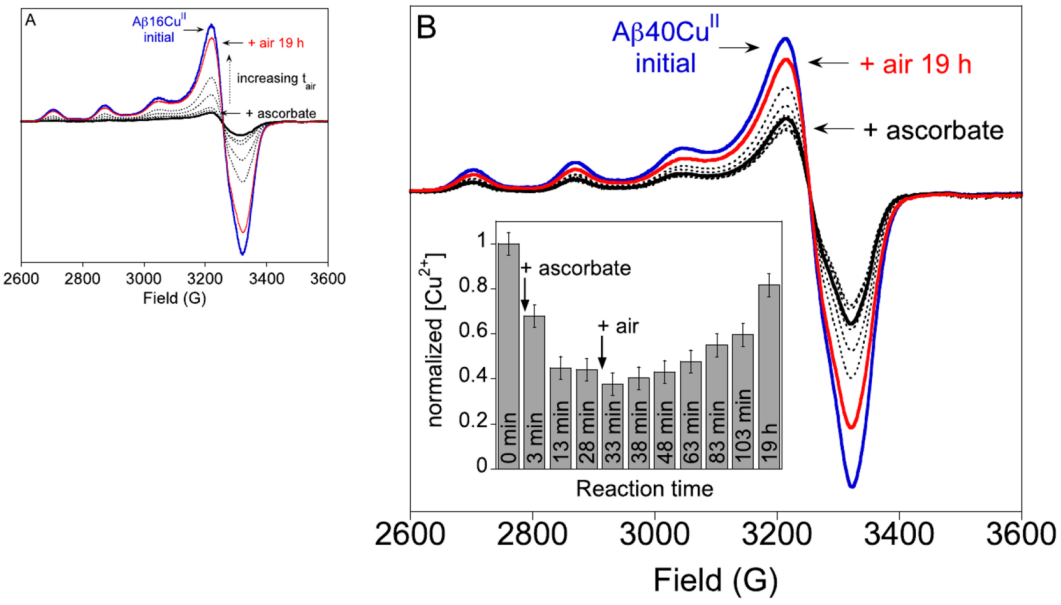

Figure 3.

20 K EPR spectra of the reduction of AβCu^{II} by ascorbate and subsequent re-oxidation in air. (A) 250 μM Aβ16Cu^{II} (blue) + 1.2 equiv ascorbate (solid black line) followed by addition of air (dotted lines, red line). (B) 100 μM Aβ40Cu^{II} (blue) + approximately 0.5 equiv ascorbate (solid black line) followed by addition of air (dotted lines, red line). Panel (B) inset, normalized Aβ40Cu^{II} signal area as a function of total reaction time. EPR conditions are given in the Materials and Methods Section.

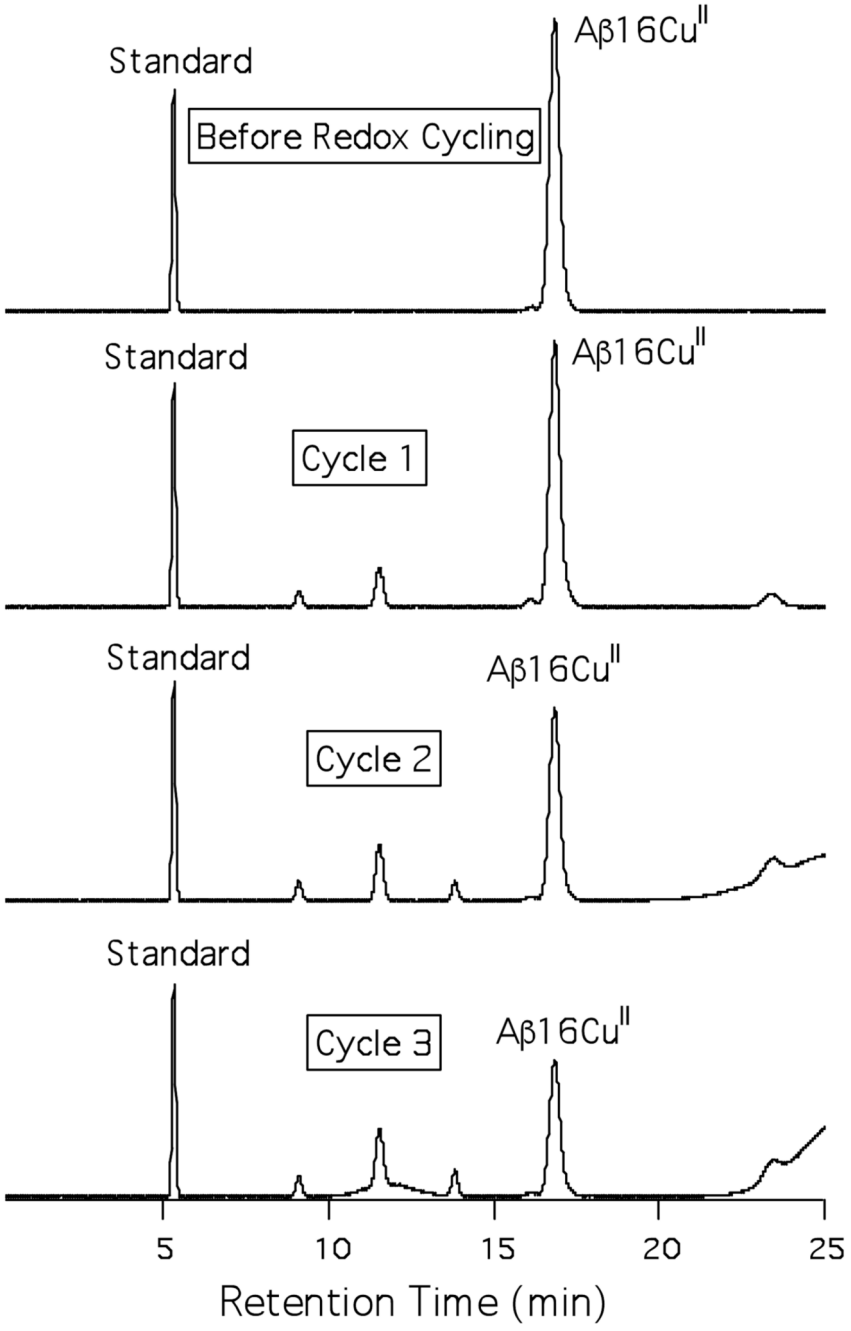

Figure 4.
HPLC chromatograms of Aβ16Cu^{II} following multiple redox cycling using ascorbate in air.

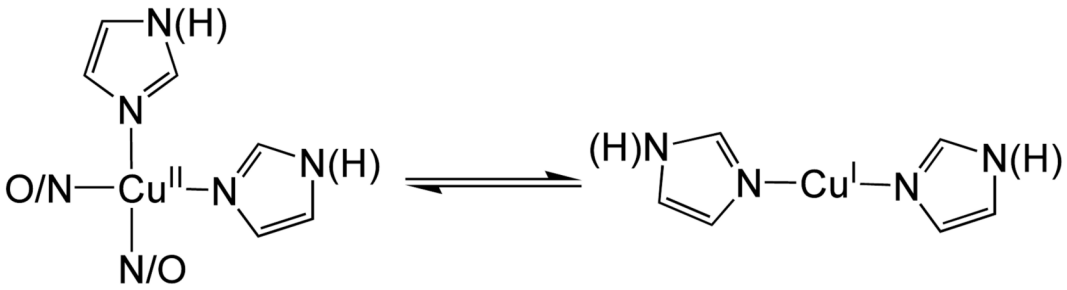

Scheme 1.

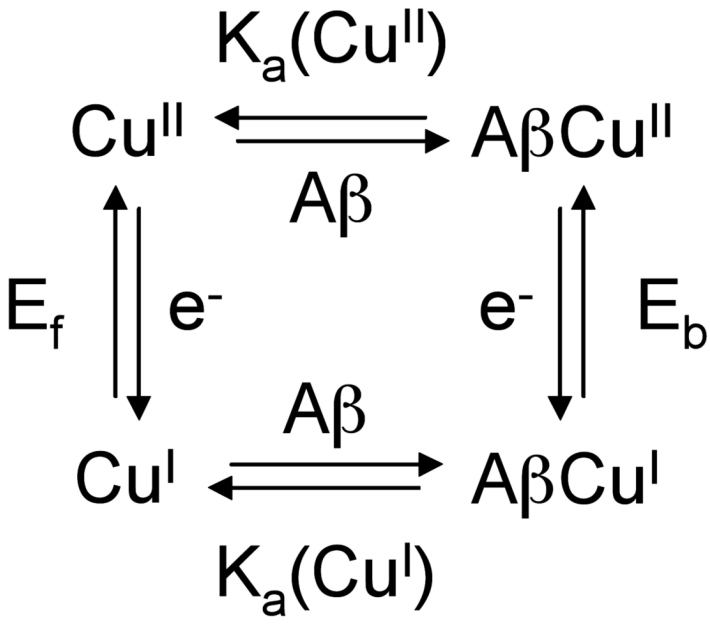

$$E_b - E_f = 0.059 \times \log\left(\frac{K_a(Cu^I)}{K_a(Cu^{II})}\right)$$

Scheme 2.

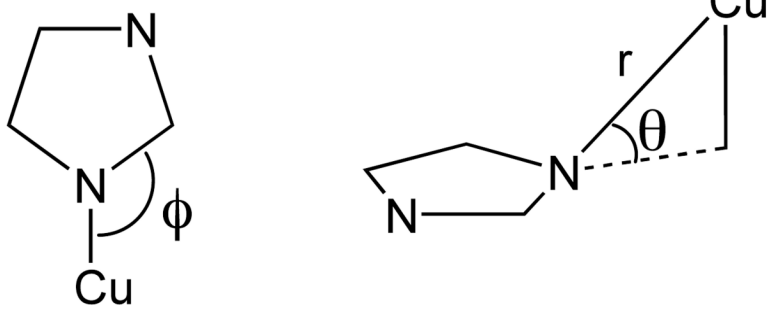

Chart 1.

Table 1

Parameters used for the refinements to the Cu K-edge X-ray Absorption data for Aβ16Cu^{II} and Aβ16Cu^{I}.

	Aβ16Cu^{II}	Aβ16Cu^{I}
Pre-edge Peak #1 (eV)	8979.3(7)	8984.1(2)
Pre-edge Peak #2 (eV)	8984.0(6)	----
E_o (eV)[a]	8988.7	8982.2
N/O-shell		
n[b]	3	2
r (Å)	1.938(12)	1.877(2)
σ^2 (Å^2)	0.0030(17)	0.0038(1)
N/O-shell		
n	1	----
r (Å)	2.07(2)	----
σ^2 (Å^2)	0.001(1)	----
Im-shell		
n	2	2
r (Å)[C]	1.938	1.877
σ^2 (Å^2)	0.003(2)	0.0057(1)
θ	8(3)°	2(2)°
ϕ	129(8)°	130(11)°
GOF	0.54	0.22
BVS	2.05	0.94

[a] For both refinements E_O was initially refined for the N-shell and then restrained.

[b] Because of the way in which the MS pathways for the Im-shell were constructed, the first N/O shell contains the SS pathway for the Im-shell. Therefore, the number of non-imidazole N/O scatterers is equal to the number of N/O scatterers in the first N/O shell minus the number of imidazole scatterers.

[c] The distance of the imidazole shell was restrained to the distance of the first N/O scatterer.